foods

MDPI

Article

Electrospray-Assisted Fabrication of Dextran–Whey Protein Isolation Microcapsules for the Encapsulation of Selenium-Enriched Peptide

Jiangling He [1,†], Zhenyu Wang [1,2,†], Lingfeng Wei [1], Yuanyuan Ye [1,2], Zia-ud Din [3], Jiaojiao Zhou [1], Xin Cong [1], Shuiyuan Cheng [1] and Jie Cai [1,2,*]

[1] National R&D Center for Se-Rich Agricultural Products Processing, Hubei Engineering Research Center for Deep Processing of Green Se-Rich Agricultural Products, School of Modern Industry for Selenium Science and Engineering, Wuhan Polytechnic University, Wuhan 430023, China
[2] Key Laboratory for Deep Processing of Major Grain and Oil, Ministry of Education, Hubei Key Laboratory for Processing and Transformation of Agricultural Products, Wuhan Polytechnic University, Wuhan 430023, China
[3] Department of Food Science and Nutrition, Women University Swabi, Swabi 23430, Khyber Pakhtunkhawa, Pakistan
* Correspondence: caijievip@whpu.edu.cn
† These authors contributed equally to this work.

Abstract: Selenium-enriched peptide (SP, selenopeptide) is an excellent organic selenium supplement that has attracted increasing attention due to its superior physiological effects. In this study, dextran–whey protein isolation–SP (DX-WPI-SP) microcapsules were fabricated via high-voltage electrospraying technology. The results of preparation process optimization showed that the optimized preparation process parameters were 6% DX (w/v), feeding rate Q = 1 mL/h, voltage U = 15 kV, and receiving distance H = 15 cm. When the content of WPI (w/v) was 4–8%, the average diameter of the as-prepared microcapsules was no more than 45 µm, and the loading rate for SP ranged from ~46% to ~37%. The DX-WPI-SP microcapsules displayed excellent antioxidant capacity. The thermal stability of the microencapsulated SP was improved, which was attributed to the protective effects of the wall materials for SP. The release performance was investigated to disclose the sustained-release capacity of the carrier under different pH values and an in-vitro-simulated digestion environment. The digested microcapsule solution showed negligible influence on the cellular cytotoxicity of Caco-2 cells. Overall, our work provides a facile strategy of electrospraying microcapsules for the functional encapsulation of SP and witnesses a broad prospect that the DX-WPI-SP microcapsules can exhibit great potential in the food processing field.

Keywords: selenium-enriched peptide; microcapsule; electrospray; release performance; cytotoxicity evaluation

check for updates

Citation: He, J.; Wang, Z.; Wei, L.; Ye, Y.; Din, Z.-u.; Zhou, J.; Cong, X.; Cheng, S.; Cai, J. Electrospray-Assisted Fabrication of Dextran–Whey Protein Isolation Microcapsules for the Encapsulation of Selenium-Enriched Peptide. *Foods* **2023**, *12*, 1008. https://doi.org/10.3390/foods12051008

Academic Editor: Jayani Chandrapala

Received: 6 December 2022
Revised: 2 February 2023
Accepted: 8 February 2023
Published: 27 February 2023

Copyright: © 2023 by the authors. Licensee MDPI, Basel, Switzerland. This article is an open access article distributed under the terms and conditions of the Creative Commons Attribution (CC BY) license (https://creativecommons.org/licenses/by/4.0/).

1. Introduction

Selenium (Se) is an indispensable micronutrient for human health. In nature, Se is mainly present in two forms, which are inorganic selenium (selenite, sodium selenite) and organic selenium (seleno amino acids, selenium polysaccharides, selenoproteins, etc.) [1]. Organic selenium has the superiorities of lower toxicity and higher bioavailability compared to inorganic selenium. Organic selenium is also much safer and can be used as a nutritional supplement for selenium-deficient people. Previous studies have claimed that the intake of super-nutritional selenium can fight cancer [2]. Therefore, people in selenium-deficient areas can select selenium-rich foods as dietary additives to keep healthy. Plant-derived selenium-enriched peptide (SP, selenopeptide) has a high biological activity, and this superiority makes it an important source of selenium supplements. The intake of SP can endow the human body with many biological effects, such as antioxidant agents [3],

fighting cancer [4], fighting inflammation [5], and immune regulation [6]. However, SP is unstable, easily denatured, and inactivated under the stimulation of oxygen, heat, alkali, etc. It is necessary to overcome these weaknesses to cater to food and other applications.

Microencapsulation has been utilized to protect functional ingredients from harsh factors [7]. The unstable matter is encapsulated within polymers to form a composite to protect the matter from the external environment. Microencapsulation technology can overcome these problems and promote applications in the food field, such as the encapsulation of fats/oil [8,9], vitamins [10], minerals [11], and biologically active substances [12–14]. The methods to construct microcapsules are mainly divided into chemical methods (in-situ polymerization, interfacial polymerization, complex coacervation), physical methods (air suspension method, spray drying method), and physical–chemical methods (sol-gel encapsulation method, supercritical CO_2-assisted method) [15]. Ko et al. prepared sulforaphane microcapsules via freeze-drying with poly(D,L-lactide-co-glycolide) as the wall material for osteoarthritis treatment [16], but the residual toxic solvents can seriously impede the applications.

Electrospraying technology can be used to prepare microparticles or nanoparticles via an electrohydrodynamic jet [17]. In recent years, it has been regarded as a direct and common method to fabricate nanoparticles and microparticles [18–20]. Compared with traditional technologies, electrospraying technology has the advantages of high efficiency and high yield. The electrospraying technology relies on a physical electric field to fabricate microcapsules without the use of heat, where the activity of functional ingredients can be well maintained. Thus, this technology is an excellent tool for encapsulating heat-sensitive substances. The as-prepared particles via electrospraying technology have uniform and controllable size distribution, good repeatability, and high production efficiency. Therefore, more attention has been paid to the research of electrospraying for the embedding and delivery of active substances [21–23]. Electrospraying technology has been used for the biopolymer encapsulation of functional food extracts to enhance their stability [24]. Costamagna et al. reported that a Chañar extract, rich in polyphenols, was encapsulated into the zein shell by electrospraying, where the stability of the extract was significantly improved [25]. Similarly, Mahalakshmi et al. prepared microcapsules via electrospraying technology to effectively embed β-carotene into zein to enhance its stability against surrounding environments [26].

Electrospraying is a gentle treatment method, which is similar to electrospinning technology, and an electrospraying device generally consists of three parts: (1) an injection module (syringe and syringe pump); (2) a high-voltage generator connected to a syringe needle for generating high voltage; (3) a receiving module (titanium alloy plate, rotating titanium alloy receiving rod or receiving solution). For the electrospraying process, it is essential to use a polymer with good solubility. Whey protein isolation (WPI) is a kind of excellent water-soluble and food-grade material with high nutrition. In addition, WPI has the potential to be used as functional encapsulation and a controlled-release delivery system due to its easily functional property and excellent biocompatibility [27]. However, excessive dissolution is a major challenge for some bioactive compounds. Dextran (DX) is an electroneutral and water-soluble polysaccharide with numerous physiological effects. Reported work has demonstrated that the introduction of DX can delay the dissolution rate of protein [28]. The interaction between proteins and polysaccharides can improve the structure, stability, encapsulation, and other specific functional properties [29]. Moreover, there are rare reports on interactions between proteins and non-charged polysaccharides. The interaction mechanism between proteins and uncharged polysaccharides is still not clear, especially regarding the ternary composite system (DX, WPI, and SP). Therefore, the study of the physicochemical properties and controlled-release properties of protein–peptide–polysaccharide ternary composite microcapsules is significant for exploring the potential prospects of SP in food fields.

Herein, electrospraying technology is employed to fabricate ternary composite microcapsules composed of DX and WPI as the wall material and SP as the core material. The utilized parameters to prepare DX-WPI-SP microcapsules are as follows: 6% DX, feeding

rate (Q) 1.0 mL/h, voltage (U) 15 kV, and receiving distance (H) 15 cm. The physicochemical properties of these ternary (DX-WPI-SP) microcapsules are investigated, and their antioxidant capacities are also analyzed. Subsequently, the preparation process is optimized to obtain DX-WPI-SP microcapsules with a higher loading rate and a smaller and more uniform particle size distribution. The release properties of the microcapsules are evaluated through the fitting of four common release models (zero order, first order, Higuchi, and Korsmeyer–Peppas) under different pH value environments (pH 2.0, pH 7.0, and pH 12.0). Furthermore, the release behavior of the DX-WPI-SP microcapsules in the simulated human digestive fluid is explored, and the biotoxicity of post-digestive ternary microcapsules is assessed. The DX-WPI-SP microcapsules exhibit great gastrointestinal dissolution characteristics and controllable release properties for SP. This work focuses on the construction of an efficient vehicle to deliver and release SP and then excavates the potential of SP as a novel selenium supplement in the food industry.

2. Materials and Methods

2.1. Materials and Reagents

Materials and reagents are recorded in the supplementary materials.

2.2. Characterizations

The main characterizations and instruments are presented in the supplementary materials.

2.3. Preparation of DX-WPI-SP Microcapsules

High-voltage electrospraying technology was used to prepare the microcapsules. The high-voltage electrospraying device was composed of a DW-N503-1ACDF0 high-voltage DC power device, an automatic injection pump, and a receiver. The preparation process referred to the reported method of Paximada et al. with some changes [30]. Anhydrous ethanol was added to the receiver to disperse the microcapsules and to remove the water within the microcapsules. Specifically, the electrostatic spray solution was dissolved in 10 mL of DI water and transferred to a 10 mL syringe. Subsequently, this syringe was fixed on the groove of the automatic syringe pump and connected with a needle through a Teflon catheter. The needle was connected to the positive pole of the high-voltage power supply, the receiver was grounded, and both of them were placed vertically.

2.4. Antioxidant Activity Evaluation

2.4.1. DPPH Radical Scavenging Assay

DPPH scavenging capacity was based on the previous report by Zhang et al., with some changes [31]. Specifically, different microcapsule solutions were mixed with 1 mL of 0.2 mM DPPH, and then the mixed solution was incubated in the dark for 30 min. The absorbance value of the mixture was recorded by the UV–vis spectrophotometer at 517 nm. The DPPH free radical scavenging rate calculation formulation is presented in the supplementary materials.

2.4.2. ABTS Radical Scavenging Ability Assay

The free radical ABTS scavenging ability of the microcapsules was evaluated following the work reported by Sridhar et al., with some modifications [32]. Specifically, the ABTS radical stock solution was produced by mixing ABTS aqueous solution (7.0 mM) with a 4.80 mM aqueous solution of potassium persulfate in equal volumes. After that, the mixture was left to react for 16 h in the dark. The ABTS stock solution was diluted to an optical density (OD) at 0.700 ± 0.001 at the optical length of 1 cm, which was defined as the ABTS work solution. The sample was poured into a 10 mL centrifuge tube, and then fresh ABTS work solution (3.8 mL) was added. The mixed solution was shaken and stood in the dark for 6 min. The absorbance value of the resultant supernatant was recorded

at 734 nm. The ABTS free radical scavenging rate calculation formulation is presented in the supplementary materials.

2.5. Stability of DX-WPI-SP Microcapsules against pH Changes

The stability of active substances can be improved after being encapsulated in microcapsules under various pH changes [33]. Herein, the pH stability of DX-WPI-SP microcapsules was evaluated by investigating the release rate of SP under different pH values and plotting the cumulative release rate curve. Specifically, 200 mg of DX-WPI-SP microcapsules were mixed with 10 mL of phosphate buffered solution with different pH and placed in a 25 mL glass bottle; 2 mL of the solution was taken out from the mixed solution at 5, 10, 30, 60, 90, and 120 min, respectively. The microcapsule suspension was centrifuged at 12,000 rpm for 2 min; 1 mL of the supernatant was taken out to determine the total selenium content through the atomic fluorescence spectrometer. The reference curve of the release rate of SP was calculated to describe the relationship between the SP concentration and the release time. All experiments were carried out in triplicate.

Mathematical models were utilized to better explain the release behavior of active substances. The zero order model and the first order model can be applied to describe the release behavior of the water-soluble components in water surroundings [34,35]. The Higuchi kinetic model is used to explain the water dissolution behavior of active substances in the solid and semi-solid matrix, and the Korsmeyer–Peppas kinetic model is usually applied to analyze the release mechanism of active substances from polymeric particle systems [36,37]. Herein, to evaluate the release mechanism of SP, multiple sustained-release kinetic models, as described above, were used to fit the release trend of DX-WPI-SP microcapsules based on the reported work [38]. The formulas are presented in the supplementary materials.

2.6. Determination of In Vitro Release Properties of DX-WPI-SP Microcapsules

Gastric digestion and intestinal digestion were performed following the method reported by Gawlik-Dziki et al., with minor modifications [39]. Simulated gastric juice was prepared by adding 3.2 g of pepsin into 0.3 M of NaCl aqueous solution, with a pH value of 1.2, using 10% of HCl solution (w/v). Simulated intestinal juice was prepared by dissolving 0.35 g of trypsin and 0.3 g of bile in 35 mL of $NaHCO_3$ aqueous solution (0.1 mol/L). The DX-WPI-SP microcapsules were incubated in the simulated gastric juice at 37 °C for 2 h and then introduced to the simulated intestinal juice for another 3 h. During the incubation, the amount of released SP in the supernatant was measured at different time intervals to calculate the release rate of SP. All experiments were conducted in triplicate.

2.7. Cell Culture and Vitality Assay In Vitro

The cytotoxicity of DX-WPI-SP microcapsules in the cell line Caco-2 (human colonic cancer cell line) was evaluated after digestion. Caco-2 was maintained in the DMEM medium containing 1% penicillin–streptomycin (PS) solution and 10% fetal bovine serum (FBS) at 37 °C in a humidified environment of 5% CO_2 and 95% air [40]. Briefly, the Caco-2 cells were adhered at a density of 5.0×10^4 cells/plate and cultured for 2–3 days. Then, the cells were sub-cultured in the same type of plate after trypsinization treatment.

A cell vitality assay was performed, referring to the reported method [41,42]; 100μL of Caco-2 cell suspension at a density of 5×10^4 cells/mL were adhered in a sterile 96-well plate to incubate for 24 h at 37 °C in a humidified environment of 5% CO_2 and 95% air. Then, 10 μL of different concentrations of digested DX-WPI-SP microcapsule solution was added. Cell viability was conducted using the CCK-8 cell proliferation and cytotoxicity assay kit. Briefly, 10 μL of 2-(2-methoxy-4-nitrophenyl)-3-(4-nitrophenyl)-5-(2,4-disulfobenzene)-2H-tetrazole monosodium salt (WST) was added into a 96-well plate for incubation for 2 h. Then, the absorbance at 450 nm was recorded with a 96-well plate reader, and 6 parallel duplicate wells were set for each concentration. The cell viability calculation formula is presented in the supplementary materials.

2.8. Statistical Analysis

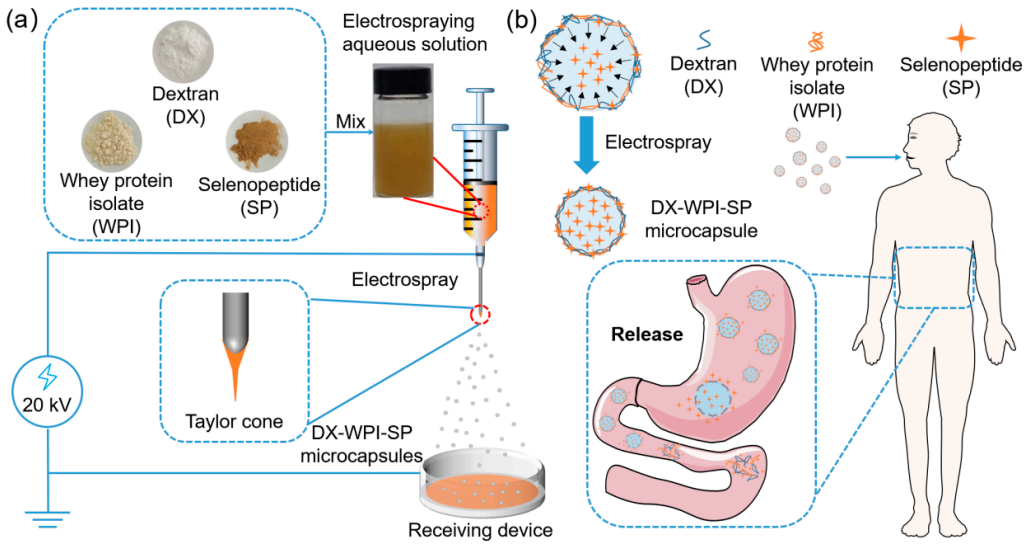
All data were presented as mean ± standard deviation (SD). Duncan's test was carried out to determine the significance of differences among the mean values ($p < 0.05$ was considered a significant level) via the SPSS Statistics 26 software program (SPSS, Inc., an IBM Company, Chicago, IL, USA).

3. Results and Discussion

3.1. Preparation of DX-WPI-SP Microcapsules

The preparation process of DX-WPI-SP microcapsules is shown in Scheme 1. DX-WPI-SP microcapsules were fabricated via high-voltage electrospray using DX and WPI as shells, loaded with SP. The fitting of the electrohydraulic kinetic process depends on the properties of the polymer solution and the operation parameters [43]. The results of the optimization of DX-WPI-SP microcapsules are presented in Figures S1–S5. The specific preparation process parameters and obtained diameters are shown in Table 1. The following parameters were summarized after the process optimization: 6% of DX (w/v), feeding rate (Q) 1.0 mL/h, applied voltage (U) 15 kV, and receiving distance (H) 15 cm. The gradual addition of WPI resulted in a mildly increasing diameter, and the decreasing loading rate of the microcapsules is shown in Figure 1. The DX-WPI-SP microcapsules obtained with these fabrication parameters have a spherical appearance and uniform size distribution (~40.06–~44.22 μm); the corresponding loading rate for SP ranged from ~46% to ~37% when the content of WPI (w/v) was 4–8%. The total Se content of the DX-WPI-SP microcapsules was calculated by referring to the standard curve, as shown in Figure S6.

The electrospraying solution ejected from the nozzle was subjected to numerous forces, including gravity and body forces (electrodynamic force, multidirectional stress, surface tangential stress, etc.). Under these comprehensive functions, the meniscus was destroyed and deformed to form a cone (Taylor cone). In addition, the electrospraying solution with free charge was accelerated and concentrated at the tip of the Taylor cone under the action of a potential difference and formed a jet, which was subsequently split into micro-scale droplets [18,44].



Scheme 1. Schematic illustration of (**a**) the preparation process of DX-WPI-SP microcapsules and (**b**) the delivery system of DX-WPI-SP microcapsules in the human gastrointestinal tract.

Table 1. Operation parameters for various microcapsules via electrospraying and the diameter of as-prepared microcapsules.

Microcapsule	DX (g)	WPI (g)	SP (g)	Voltage (kV)	Distance (cm)	Feeding Rate (mL/h)	Diameter (μm)
DX microcapsules	0.6	-	-	15	15	1.0	26.47 ± 3.50
DX-WPI microcapsules	0.6	0.2	-	15	15	1.0	30.31 ± 2.91
	0.6	0.4	-	15	15	1.0	30.75 ± 3.64
	0.6	0.6	-	15	15	1.0	33.42 ± 3.09
	0.6	0.8	-	15	15	1.0	34.38 ± 4.07
	0.6	1.0	-	15	15	1.0	35.83 ± 3.64
DX-WPI-SP microcapsules	0.6	0.4	0.9	15	15	1.0	40.06 ± 5.25
	0.6	0.6	0.9	15	15	1.0	41.65 ± 4.37
	0.6	0.8	0.9	15	15	1.0	44.22 ± 4.75

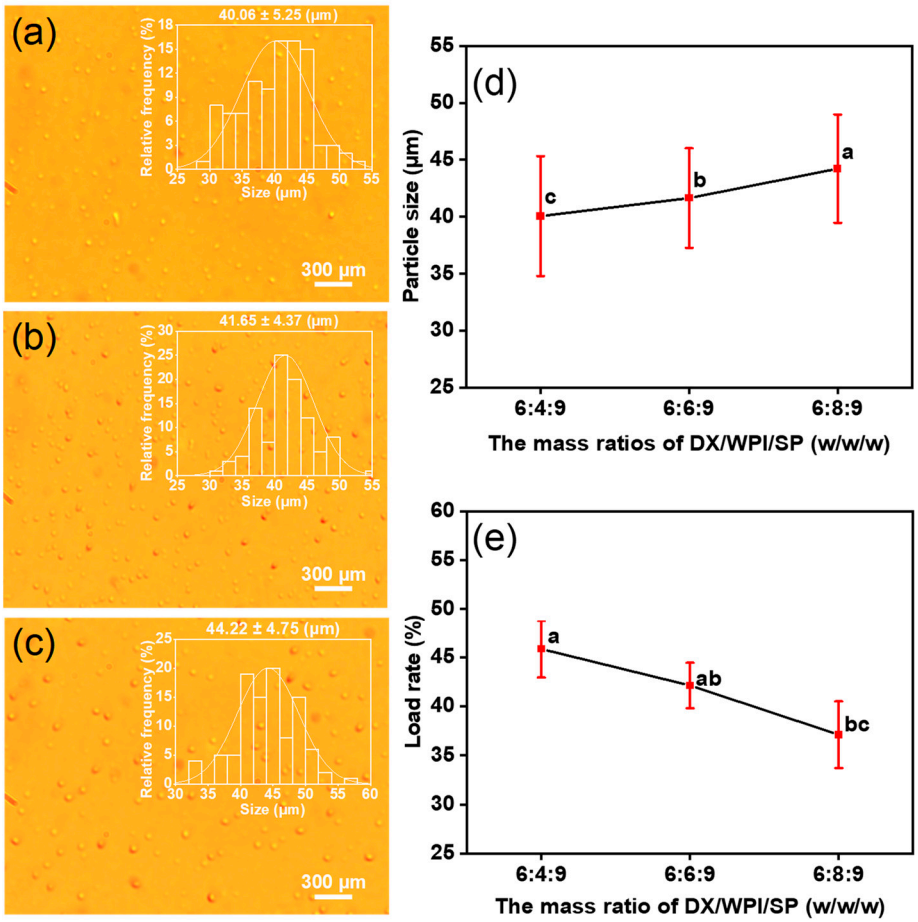


Figure 1. (**a**–**c**) Optical images and particle size distribution of DX-WPI-SP microcapsules with different DX/WPI/SP mass ratios (a—6:4:9, b—6:6:9, c—6:8:9). (**d**) The average particle size and (**e**) the average loading rate of these DX-WPI-SP microcapsules against different mass ratios of DX/WPI/SP (6:4:9, 6:6:9, 6:8:9, *w*/*w*/*w*). Different letters represent significant differences between groups by Duncan's test ($p < 0.05$).

3.2. Structure and Characterization of DX-WPI-SP Microcapsules

Figure 2 shows the scanning electron microscope (SEM) images of DX microcapsules, DX-WPI microcapsules, and DX-WPI-SP microcapsules for surface morphology observation. Figure 2a shows that the pure DX microcapsules appear to have a smooth surface. However, Figure 2b shows that the DX-WPI microcapsules are irregularly shaped, with a rough surface. This is because the receiving solvent (anhydrous ethanol) grabs a lot of

water within a short duration, resulting in the rough surface of the microcapsules and many voids after the ethanol reaches the microcapsules. Compared with the SEM image of DX-WPI microcapsules, there are more bumps and folds on the surface of the DX-WPI-SP microcapsules (Figure 2c).

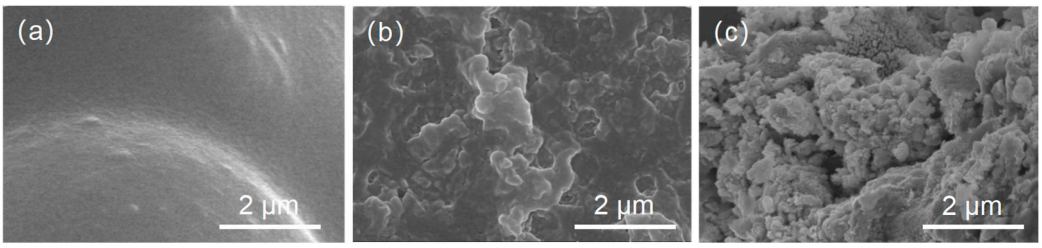


Figure 2. SEM images of (**a**) DX microcapsules, (**b**) DX-WPI microcapsules, and (**c**) DX-WPI-SP microcapsules.

FTIR was used to further identify the chemical bonding function and to characterize interactions between the functional groups of DX microcapsules, DX-WPI microcapsules, DX-WPI-SP microcapsules, WPI, and SP. The FTIR spectrum (Figure 3a) showed a characteristic peak at ~1640 cm^{-1}, which is ascribed to the C=O stretching vibration within the amide I band. The characteristic peak at ~1590 cm^{-1} can be assigned to C-N stretching vibration in the amide II band [45]. The regions at 1000–1250 and 1300–1400 cm^{-1} indicate the existence of C-N and C-O bonds [46,47]. The FTIR spectrum of DX revealed a peak at ~3368 cm^{-1}, which is due to the presence of -OH. After SP microencapsulation, a redshift from ~3300 to ~3286 cm^{-1} of this peak was noted for DX-WPI-SP microcapsules, which could be attributed to the enhancement of the hydrogen bond and a decreased number of free hydroxyl groups [48]. Therefore, the DX-WPI-SP microcapsules have a more compact structure. The peak at ~1271 cm^{-1} can be assigned to C-O, and the regions at ~917 and ~765 cm^{-1} are characteristic peaks from dextran [49]. In addition, all characteristic peaks of SP, DX, and WPI appeared in the FTIR spectrum of the DX-WPI-SP microcapsules, which provided good evidence that the SP was successfully loaded onto the DX-WPI microcapsules. It was notable that no new peaks appeared in the FTIR spectrum of the DX-WPI-SP microcapsules, suggesting that no new chemical bond was formed between DX-WPI and SP, and DX-WPI was used as the SP carrier without significant change to its inherent properties.

X-ray diffraction (XRD) was used to analyze the crystal phase of the substances. As shown in Figure 3b, the SP source had characteristic peaks at ~11.7°, ~20.8°, ~29.1°, ~31.2°, and ~33.4°, indicating the SP has a crystalline nature. XRD patterns of the DX microcapsules showed that the peak at 2θ = ~18.9° was broad and round, exhibiting that the DX microcapsules were amorphous [50]. After DX microcapsules were complexed with WPI, a new peak appeared at 2θ = ~8.9°, which was attributed to the addition of WPI. The XRD pattern of the DX-WPI-SP microcapsules revealed that this compound was mainly amorphous. All typical bands of the DX-WPI microcapsules remained within the XRD pattern of the DX-WPI-SP microcapsules.

To investigate the thermal stability and degradation process, the thermal stability of DX microcapsules, DX-WPI microcapsules, and DX-WPI-SP microcapsules, as well as SP, was evaluated with TGA under a nitrogen atmosphere. The TGA and DTG thermograms are shown in Figure 3c,d. In Figure 3c, all substances exhibit a typical two-step thermal degradation process in their TGA thermograms. The first stage is with a minor weight loss, which is attributed to the loss of moisture. The second stage shows a heavy weight loss as a result of the thermal decomposition of the chemical compounds [51]. The degradation rate of the DX-WPI microcapsules was lower than that of the DX microcapsules, which maybe due to the improved heat resistance of the backbone network in the compound because of the enhancement of interactions between proteins and polysaccharides, such as hydrophobic interactions and hydrogen bonding functions. Figure 3d shows that free SP has a clear heat degradation process from ~120 to ~300 °C. However, after microencapsulation, the degradation

rate is significantly slowed down, which is coincident with the fact that the wall material can protect the SP against thermal degradation and improve its thermal stability. Researchers have also found that the thermal stability of squalene was improved after encapsulation treatment by polysaccharide and protein comparing to that of pure squalene [52].

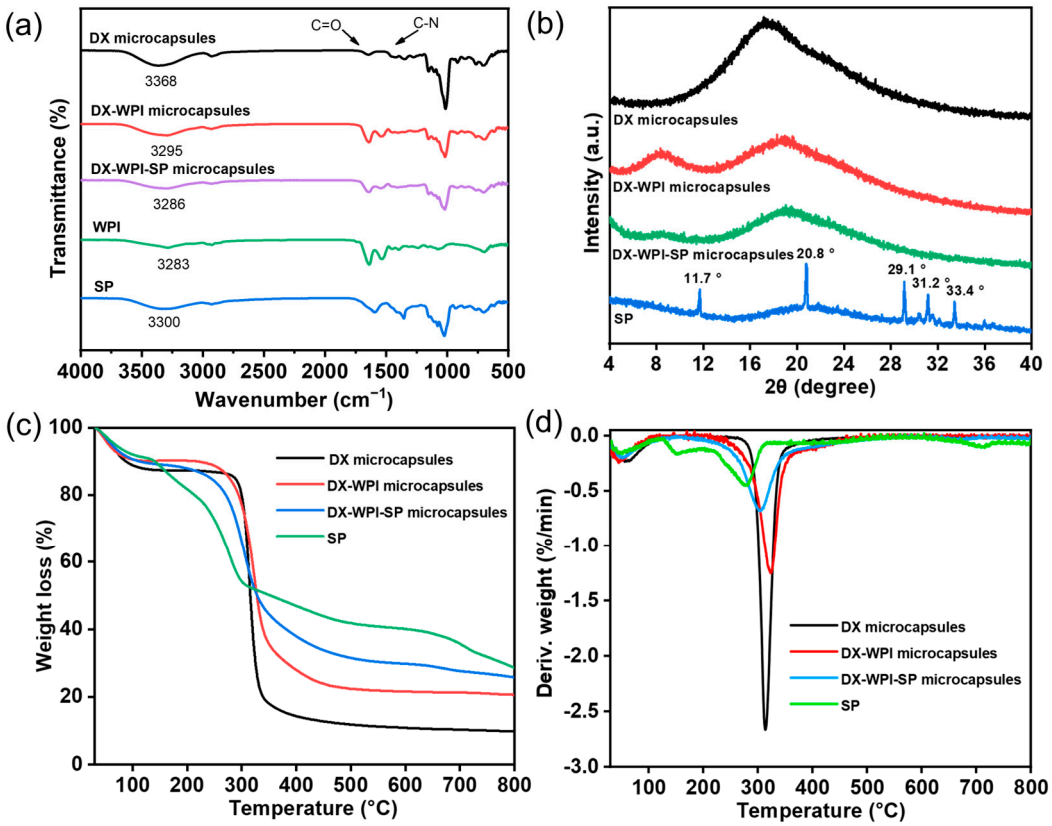


Figure 3. (**a**) FTIR curves, (**b**) XRD patterns, (**c**) TGA curves, and (**d**) DTG curves of DX microcapsules, DX-WPI microcapsules, DX-WPI-SP microcapsules, WPI, and SP.

3.3. Antioxidant Activity Evaluation of DX-WPI-SP Microcapsules

The DPPH free radical scavenging test and the ABTS free radical scavenging test were used to evaluate the antioxidant properties of substances. Figure 4a,b show the DPPH and ABTS free radical scavenging rates of SP under different mass concentrations. SP exhibited increasing DPPH and ABTS free radical scavenging activities with the gradual introduction of SP. Figure 4c,d show the DPPH and ABTS radical scavenging activity comparisons of DX microcapsules, DX-WPI microcapsules, DX-WPI-SP microcapsules, and SP, respectively. The antioxidant activity of DX-WPI-SP microcapsules was only ~67.7% of that of free SP. It was noteworthy that the antioxidant activity of DX-WPI-SP microcapsules was significantly higher than that of both DX microcapsules and DX-WPI microcapsules. The complexation of SP could enhance the antioxidant activity of the DX-WPI microcapsules, and the DX-WPI-SP microcapsules had excellent antioxidant capacity.

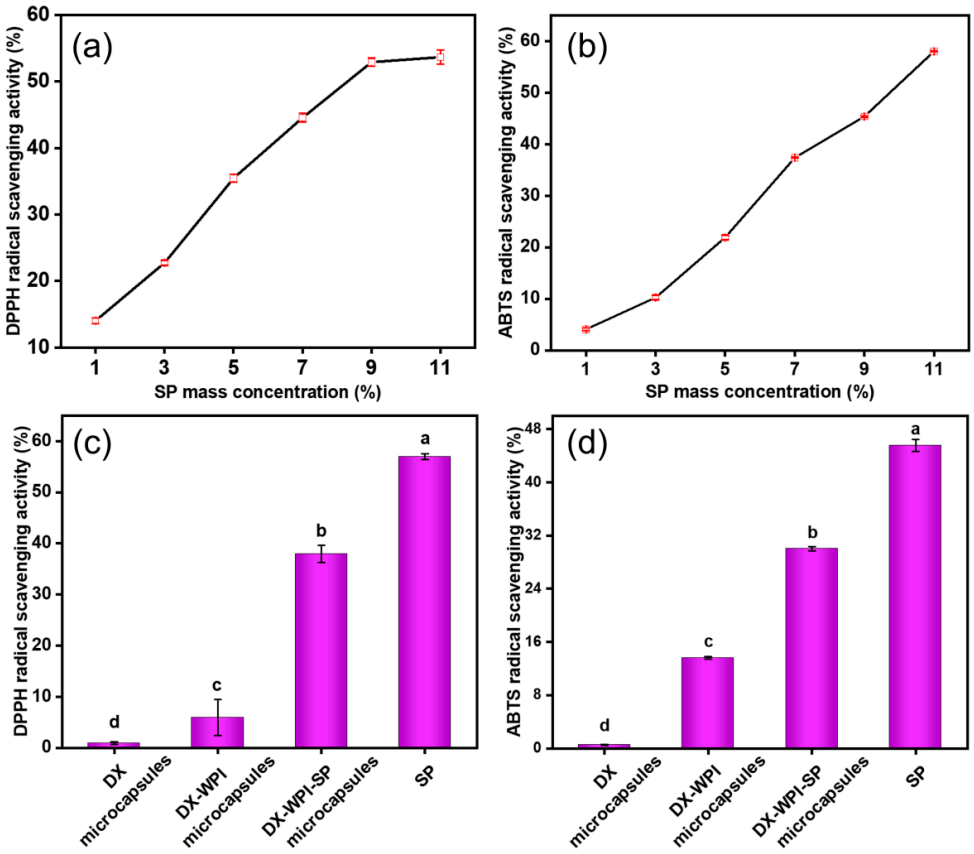


Figure 4. (**a**) DPPH and (**b**) ABTS radical scavenging activity against various SP concentrations. (**c**) DPPH and (**d**) ABTS radical scavenging activity comparisons of DX microcapsules, DX-WPI microcapsules, DX-WPI-SP microcapsules, and SP (all of them were 9%, w/v). Different letters represent significant differences between columns by Duncan's test ($p < 0.05$).

3.4. Controlled-Release Properties Evaluation Results

Figure 5a shows the release behavior of DX-WPI-SP microcapsules under different pH conditions (pH 2.0, pH 7.0, and pH 12.0). The SP was rapidly released from the DX-WPI-SP microcapsules within 10 min, with a release rate of 70–80%, and then the release rate increased slowly and held steady. The release rate of the SP from the DX-WPI-SP microcapsules was faster in the initial release stage, resulting in a large accumulated SP content. As the infiltration process was delayed, the release rate of SP gradually slowed down and held steady at about 70–85%. The SP was more easily released from the encapsulated microcapsules at lower pH values, where the DX-WPI wall material was more easily collapsed. Similar phenomena occurred in alginate-whey protein isolate microcapsules [53]. The strong basic environment affected non-covalent interactions within the WPI, including van der Waals force, hydrophobic interaction, hydrogen bonding function, etc. [54]. In strong basic surroundings, the DX-WPI wall was harder to disintegrate from DX-WPI-SP compared to acidic environments, which was attributed to the excessive exposure of the hydrophobic groups of WPI [55]. The enhancement of hydrophobic interactions decreased the solubility of WPI and led to its aggregation in water environments [56,57]. Thus, the release rate of SP from DX-WPI-SP microcapsules was lower at the higher pH values, and the DX-WPI-SP microcapsules could also show controllable release properties for SP.

The release mechanism model for active substance release can essentially reveal the influence of release dynamics and release architecture variables [38]. Diffusion, swelling, and erosion are the main release processes that affect the control and release behaviors of the active ingredients. The higher the local activated material concentration, the faster the diffusion efficiency of SP from the DX-WPI-SP microcapsules. Similar results were reported

by Ge et al. and Wu et al. [58,59]. The kinetic parameters are shown in Table S1 for the release process of SP from DX-WPI-SP microcapsules in different pH values, and the results of the fitting of release kinetics are presented in the supplementary materials.

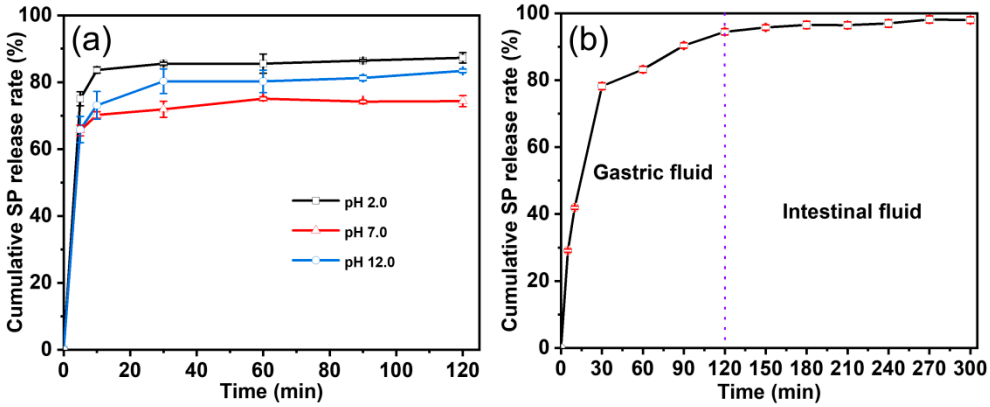


Figure 5. The cumulative release curves of SP released from DX-WPI-SP microcapsules under (**a**) the different pH values (pH 2.0, pH 7.0, and pH 12.0) and (**b**) the simulated gastric and intestinal digestion surroundings.

The release performance of SP from the DX-WPI-SP microcapsules was monitored in the simulated gastrointestinal tract (Scheme 1). As shown in Figure 5b, the SP was rapidly released within 120 min, with a release rate of ~90%, which is consistent with the release behavior of SP from the DX-WPI-SP microcapsules under acidic conditions (pH 2.0) (Figure 5a). The conformational change of WPI under acidic conditions can make pepsin more accessible to targets with amino acid residues, and the enzymatic hydrolysis of WPI can increase the release of SP. Nongonierma et al. gathered the similar result that the release rate of bioactive peptides was enhanced via enzymatic hydrolysis of milk proteins [60].

3.5. Cytotoxicity Study of Digested DX-WPI-SP Microcapsules

The cellular cytotoxicity of DX-WPI-SP microcapsules by the treatment of a digestive solution for Caco-2 cells was determined by the CCK-8 kit. As shown in Table 2, the Se content showed a negligible influence on the cellular cytotoxicity of Caco-2 cells, where the cell viability was still over 90% even when the Se content was up to ~46 μg/mL. Therefore, it is implied that DX-WPI-SP microcapsules have quite low toxicity and great biocompatibility, and they also show potential as selenium supplements and are an excellent prospect in the food field.

Table 2. Cytotoxicity of digestive solutions at different dilutions.

Digestive Solution at Different Dilutions	Total Selenium Content (μg/mL)	Cell Viability (%)	*p* Value [a]
Control	-	100	-
Digestive solution	45.72 ± 2.98	97.21 ± 2.57 [a]	0.9127 [ns]
Digestive solution-2	22.86 ± 1.49	98.33 ± 2.90 [a]	0.9925 [ns]
Digestive solution-10	4.57 ± 0.30	95.94 ± 4.00 [a]	0.6711 [ns]
Digestive solution-20	2.29 ± 0.15	97.94 ± 5.22 [a]	0.9783 [ns]
Digestive solution-50	1.14 ± 0.06	97.58 ± 0.66 [a]	0.9533 [ns]
Digestive solution-100	0.57 ± 0.03	96.69 ± 2.93 [a]	0.8298 [ns]

[a] Duncan's significance test. [ns] $p > 0.05$ is considered as not significant compared with the control group. Digestive solution-X (2, 10, 20, 50, and 100): X represents the diluted times of the digestive solution with PBS buffer solution.

4. Conclusions

In summary, a facile strategy of a selenium-enriched peptide (SP, selenopeptide) carrier has been reported for the protection and delivery of SP. Dextran–whey protein isolation–selenopeptide (DX-WPI-SP) microcapsules were fabricated via high-voltage electrospraying technology. This work has optimized the process parameters to obtain microcapsules with

suitable particle size and high loading efficiency. The optimized process parameters include the following: concentration of dextran (DX) 6%, feeding rate 1.0 mL/h, applied voltage 15 kV, and receiving distance 15 cm. When the concentration of whey protein isolation (WPI) was 4–8%, the corresponding diameter of the DX-WPI-SP microcapsules was below 45 μm, and the loading rate for SP was in the range of ~46% to ~37%. Compared with free SP, the thermal stability of microencapsulated SP (DX-WPI-SP) was significantly improved due to the protection function of the wall materials of DX-WPI. The release properties of SP from the DX-WPI-SP microcapsules were monitored under different pH values, where the DX-WPI-SP microcapsules exhibited a controllable release effect on SP. The SP release dynamic from the microcapsules was nearly in accordance with the first order model (pH 2.0) and the Korsmeyer–Peppas model (pH 7.0 and pH 12.0). The results of in vitro simulation experiments show that the DX-WPI-SP microcapsules have excellent gastrointestinal dissolution characteristics and controllable release properties for SP. Herein, this work provides a valuable tool to fabricate and encapsulate selenium-enriched materials and also provides a vehicle for the controllable release of SP in vitro. The constructed system has outstanding biocompatibility and negligible cellular cytotoxicity, exhibiting prospects and potential in the food industry.

Supplementary Materials: The following supporting information can be downloaded at: https://www.mdpi.com/article/10.3390/foods12051008/s1, Figure S1: Optical images, particle size distribution, and average particle sizes of dextran microcapsules with different concentrations of dextran; Figure S2: Optical images, particle size distribution, and average particle sizes of dextran microcapsules with different feeding rates; Figure S3: Optical images, particle size distribution, and average particle sizes of dextran microcapsules with different voltage electrostatic spraying; Figure S4: Optical images, particle size distribution, and average particle sizes of dextran microcapsules with different receiving distances; Figure S5: Optical images, particle size distribution, and average particle sizes of DX-WPI microcapsules with different DX/WPI mass ratios; Figure S6: Standard curve for the determination of total selenium content; Table S1: Kinetic parameters for the release process of SP from DX-WPI-SP microcapsules in different pH values. References [58,59,61–66] are cited in the supplementary materials.

Author Contributions: Conceptualization, J.H. and J.C.; methodology, Z.W. and L.W.; formal analysis, Z.W. and L.W.; investigation, Z.W. and L.W.; data curation, Z.W. and L.W.; writing—original draft preparation, J.H., Z.W. and L.W.; writing—review and editing, J.H., Z.W., L.W., Y.Y., Z.-u.D., J.Z. and J.C.; visualization, J.H., Z.W., L.W. and J.C.; supervision, J.H. and J.C.; project administration, X.C., S.C. and J.C.; funding acquisition, J.C. All authors have read and agreed to the published version of the manuscript.

Funding: This research was partly funded by the Technical Reserve Project from the School of Modern Industry for Selenium Science and Engineering, Wuhan Polytechnic University, and Enshi Se-Run Material Engineering Technology Co., Ltd. (Se1-202110). Research on the functional characterization of polysaccharide-based delivery systems was partly supported by the International Science and Technology Cooperation Project of Hubei Province of China (No. 2021EHB029).

Data Availability Statement: The data presented in this study are available upon request from the corresponding author. The data are not publicly available because of privacy issues.

Acknowledgments: The authors would like to thank Enshi Se-Run Material Engineering Technology Co., Ltd. for the supply of selenium-enriched peptide powder in this study.

Conflicts of Interest: The authors declare that this study received the funding of Technical Reserve Project from the School of Modern Industry for Selenium Science and Engineering, Wuhan Polytechnic University & Enshi Se-Run Material Engineering Technology Co., Ltd. (Se1-202110). This project provided the selenium-enriched peptide powder and financial support for the finish of this study. The funder was not involved in the study design, collection, analysis, interpretation of data, the writing of this article or the decision to submit it for publication. The authors declare no conflict of interest.

References

1. Chen, N.; Zhao, C.; Zhang, T. Selenium transformation and selenium-rich foods. *Food Biosci.* **2021**, *40*, 100875. [CrossRef]
2. Raines, A.M.; Sunde, R.A. Selenium toxicity but not deficient or supernutritional selenium status vastly alters the transcriptome in rodents. *BMC Genomics* **2011**, *12*, 26. [CrossRef]
3. Zhu, S.; Du, C.; Yu, T.; Cong, X.; Liu, Y.; Chen, S.; Li, Y. Antioxidant activity of selenium-enriched peptides from the protein hydrolysate of *Cardamine violifolia*. *J. Food Sci.* **2019**, *84*, 3504–3511. [CrossRef]
4. Li, X.; Wang, X.; Liu, G.; Xu, Y.; Wu, X.; Yi, R.; Jin, F.; Sa, C.; Su, X. Antioxidant stress and anticancer of peptide chelate selenium element in vitro. *Int. J. Mol. Med.* **2020**, *48*, 1–15. [CrossRef]
5. Feng, M.; Wang, X.; Xiong, H.; Qiu, T.; Zhang, H.; Guo, F.; Jiang, L.; Sun, Y. Anti-inflammatory effects of three selenium-enriched brown rice protein hydrolysates in LPS-induced RAW264.7 macrophages via NF-κB/MAPKs signaling pathways. *J. Funct. Foods* **2021**, *76*, 104320. [CrossRef]
6. Fang, Y.; Pan, X.; Zhao, E.; Shi, Y.; Shen, X.; Wu, J.; Pei, F.; Hu, Q.; Qiu, W. Isolation and identification of immunomodulatory selenium-containing peptides from selenium-enriched rice protein hydrolysates. *Food Chem.* **2019**, *275*, 696–702. [CrossRef] [PubMed]
7. Corrêa-Filho, L.C.; Moldão-Martins, M.; Alves, V.D. Advances in the application of microcapsules as carriers of functional compounds for food products. *Appl. Sci.* **2019**, *9*, 571. [CrossRef]
8. Wehrle, K.; Gallagher, E.; Neville, D.P.; Keogh, M.K.; Arendt, E.K. Microencapsulated high-fat powders in biscuit production. *Z. Lebensm-Forsch. A* **1999**, *208*, 388–393. [CrossRef]
9. Tao, L.; Wang, P.; Zhang, T.; Ding, M.; Liu, L.; Tao, N.; Wang, X.; Zhong, J. Preparation of multicore millimeter-sized spherical alginate capsules to specifically and sustainedly release fish oil. *Food Sci. Hum. Wellness* **2023**, *12*, 397–406. [CrossRef]
10. Comunian, T.; Babazadeh, A.; Rehman, A.; Shaddel, R.; Akbari-Alavijeh, S.; Boostani, S.; Jafari, S.M. Protection and controlled release of vitamin C by different micro/nanocarriers. *Crit. Rev. Food Sci. Nutr.* **2022**, *62*, 3301–3322. [CrossRef]
11. Gomez-Betancur, A.M.; Carmona-Tamayo, R.; Martínez-Álvarez, O.L.; Casanova-Yepes, H.; Torres-Oquendo, J.D. Effect of fat substitution using long-chain inulin and fortification with microencapsulated calcium in the rheological and sensory properties of yogurt mousse. *J. Food Process. Eng.* **2020**, *45*, e13433. [CrossRef]
12. Chen, L.; Zhang, D.; Wei, L.F.; Zhu, W.J.; Yan, X.Q.; Zhou, R.; Din, Z.U.; Ding, W.P.; Ma, T.Z.; Cai, J. Structural and mechanistic insights into starch microgel/anthocyanin complex assembly and controlled release performance. *Int. J. Biol. Macromol.* **2022**, *213*, 718–727. [CrossRef] [PubMed]
13. Sun, Y.; Zhang, M.; Bhandari, B.; Bai, B. Fennel essential oil loaded porous starch-based microencapsulation as an efficient delivery system for the quality improvement of ground pork. *Int. J. Biol. Macromol.* **2021**, *172*, 464–474. [CrossRef] [PubMed]
14. Wong, C.Y.; Al-Salami, H.; Dass, C.R. Microparticles, microcapsules and microspheres: A review of recent developments and prospects for oral delivery of insulin. *Int. J. Pharm.* **2018**, *537*, 223–244. [CrossRef] [PubMed]
15. Bah, M.G.; Bilal, H.M.; Wang, J. Fabrication and application of complex microcapsules: A review. *Soft Matter* **2020**, *16*, 570–590. [CrossRef] [PubMed]
16. Ko, J.Y.; Choi, Y.J.; Jeong, G.J.; Im, G.I. Sulforaphane-PLGA microspheres for the intra-articular treatment of osteoarthritis. *Biomaterials* **2013**, *34*, 5359–5368. [CrossRef]
17. Wang, J.; Zhang, Y.; Zhang, W.; Fan, Z. Research progress of electrostatic spray technology over the last two decades. *J. Energy Eng.* **2021**, *147*, 03121003. [CrossRef]
18. Jaworek, A.; Sobczyk, A.T. Electrospraying route to nanotechnology: An overview. *J. Electrost.* **2008**, *66*, 197–219. [CrossRef]
19. Jaworek, A. Micro- and nanoparticle production by electrospraying. *Powder Technol.* **2007**, *176*, 18–35. [CrossRef]
20. Zhu, Y.; Chen, Y.; Xu, G.; Ye, X.; He, D.; Zhong, J. Micropattern of nano-hydroxyapatite/silk fibroin composite onto Ti alloy surface via template-assisted electrostatic spray deposition. *Mater. Sci. Eng. C* **2012**, *32*, 390–394. [CrossRef]
21. Wang, P.; Ding, M.; Zhang, T.; Wu, T.; Qiao, R.; Zhang, F.; Wang, X.; Zhong, J. Electrospraying technique and its recent application advances for biological macromolecule encapsulation of food bioactive substances. *Food Rev. Int.* **2022**, *38*, 566–588. [CrossRef]
22. Dhiman, A.; Suhag, R.; Singh, A.; Prabhakar, P.K. Mechanistic understanding and potential application of electrospraying in food processing: A review. *Crit. Rev. Food Sci. Nutr.* **2022**, *62*, 8288–8306. [CrossRef] [PubMed]
23. Rostamabadi, H.; Falsafi, S.R.; Rostamabadi, M.M.; Assadpour, E.; Jafari, S.M. Electrospraying as a novel process for the synthesis of particles/nanoparticles loaded with poorly water-soluble bioactive molecules. *Adv. Colloid Interface Sci.* **2021**, *290*, 102384. [CrossRef]
24. Drosou, C.G.; Krokida, M.K.; Biliaderis, C.G. Encapsulation of bioactive compounds through electrospinning/electrospraying and spray drying: A comparative assessment of food-related applications. *Dry. Technol. Int. J.* **2016**, *35*, 139–162. [CrossRef]
25. Costamagna, M.S.; Gómez-Mascaraque, L.G.; Zampini, I.C.; Alberto, M.R.; Pérez, J.; López-Rubio, A.; Isla, M.I. Microencapsulated chañar phenolics: A potential ingredient for functional foods development. *J. Funct. Foods* **2017**, *37*, 523–530. [CrossRef]
26. Mahalakshmi, L.; Leena, M.M.; Moses, J.A.; Anandharamakrishnan, C. Micro- and nano-encapsulation of beta-carotene in zein protein: Size-dependent release and absorption behavior. *Food Funct.* **2020**, *11*, 1647–1660. [CrossRef]
27. Doherty, S.B.; Gee, V.L.; Ross, R.P.; Stanton, C.; Fitzgerald, G.F.; Brodkorb, A. Development and characterisation of whey protein micro-beads as potential matrices for probiotic protection. *Food Hydrocolloids* **2011**, *25*, 1604–1617. [CrossRef]

28. Du, X.; Hu, M.; Liu, G.; Yan, S.; Qi, B.; Zhang, S.; Huang, Y.; Li, Y.; Chen, H.; Zhu, X. Development of high-internal-phase emulsions stabilized by soy protein isolate-dextran complex for the delivery of quercetin. *J. Sci. Food Agric.* **2022**, *102*, 6273–6284. [CrossRef]
29. Zhang, N.; Zhou, Q.; Fan, D.; Xiao, J.; Zhao, Y.; Cheng, K.-W.; Wang, M. Novel roles of hydrocolloids in foods: Inhibition of toxic maillard reaction products formation and attenuation of their harmful effects. *Trends Food Sci. Technol.* **2021**, *111*, 706–715. [CrossRef]
30. Paximada, P.; Kanavou, E.; Mandala, I.G. Effect of rheological and structural properties of bacterial cellulose fibrils and whey protein biocomposites on electrosprayed food-grade particles. *Carbohydr. Polym.* **2020**, *241*, 116319. [CrossRef]
31. Zhang, J.; Li, M.; Zhang, G.; Tian, Y.; Kong, F.; Xiong, S.; Zhao, S.; Jia, D.; Manyande, A.; Du, H. Identification of novel antioxidant peptides from snakehead (*Channa argus*) soup generated during gastrointestinal digestion and insights into the anti-oxidation mechanisms. *Food Chem.* **2021**, *337*, 127921. [CrossRef]
32. Sridhar, K.; Charles, A.L. In vitro antioxidant activity of Kyoho grape extracts in DPPH and ABTS assays: Estimation methods for EC_{50} using advanced statistical programs. *Food Chem.* **2019**, *275*, 41–49. [CrossRef]
33. Bustos-Garza, C.; Yáñez-Fernández, J.; Barragán-Huerta, B.E. Thermal and pH stability of spray-dried encapsulated astaxanthin oleoresin from *Haematococcus pluvialis* using several encapsulation wall materials. *Food Res. Int.* **2013**, *54*, 641–649. [CrossRef]
34. Mulye, N.V.; Turco, S.J. A simple-model based on first-order kinetics to explain release of highly water-soluble drugs from porous dicalcium phosphate dihydrate matrices. *Drug Dev. Ind. Pharm.* **1995**, *21*, 943–953. [CrossRef]
35. Laracuente, M.L.; Yu, M.H.; McHugh, K.J. Zero-order drug delivery: State of the art and future prospects. *J. Controlled Release* **2020**, *327*, 834–856. [CrossRef] [PubMed]
36. Liu, C.; Desai, K.G.H.; Tang, X.; Chen, X. Drug release kinetics of spray-dried chitosan microspheres. *Dry. Technol. Int. J.* **2007**, *24*, 769–776. [CrossRef]
37. Bohrey, S.; Chourasiya, V.; Pandey, A. Polymeric nanoparticles containing diazepam: Preparation, optimization, characterization, in-vitro drug release and release kinetic study. *Nano Converg.* **2016**, *3*, 3. [CrossRef] [PubMed]
38. Budincic, J.M.; Petrovic, L.; Dekic, L.; Fraj, J.; Bucko, S.; Katona, J.; Spasojevic, L. Study of vitamin E microencapsulation and controlled release from chitosan/sodium lauryl ether sulfate microcapsules. *Carbohydr. Polym.* **2021**, *251*, 116988. [CrossRef] [PubMed]
39. Gawlik-Dziki, U.; Dziki, D.; Baraniak, B.; Lin, R. The effect of simulated digestion in vitro on bioactivity of wheat bread with Tartary buckwheat flavones addition. *LWT-Food Sci. Technol.* **2009**, *42*, 137–143. [CrossRef]
40. Xiang, Q.; Zhang, W.; Li, Q.; Zhao, J.; Feng, W.; Zhao, T.; Mao, G.; Chen, Y.; Wu, X.; Yang, L.; et al. Investigation of the uptake and transport of polysaccharide from Se-enriched *Grifola frondosa* in Caco-2 cells model. *Int. J. Biol. Macromol.* **2020**, *158*, 1330–1341. [CrossRef]
41. Zhou, Y.; She, X.; Chen, Z.; Wei, Y.; Xiao, Y.; Zhou, X. Tartary buckwheat *(Fagopyrum tataricum* (L.) Gaertn) protein-derived antioxidant peptides: Mechanisms of action and structure-activity relationship in Caco-2 cell models. *Food Sci. Hum. Wellness* **2022**, *11*, 1580–1590. [CrossRef]
42. Ye, Y.; Li, P.; Zhou, J.; He, J.; Cai, J. The improvement of sensory and bioactive properties of yogurt with the introduction of tartary buckwheat. *Foods* **2022**, *11*, 1774. [CrossRef]
43. Pérez-Masiá, R.; Lagaron, J.M.; López-Rubio, A. Development and optimization of novel encapsulation structures of interest in functional foods through electrospraying. *Food Bioprocess Technol.* **2014**, *7*, 3236–3245. [CrossRef]
44. Guarino, V.; Altobelli, R.; Cirillo, V.; Cummaro, A.; Ambrosio, L. Additive electrospraying: A route to process electrospun scaffolds for controlled molecular release. *Polym. Adv. Technol.* **2015**, *26*, 1359–1369. [CrossRef]
45. Sadat, A.; Joye, I.J. Peak fitting applied to Fourier transform infrared and Raman spectroscopic analysis of proteins. *Appl. Sci.* **2020**, *10*, 5918. [CrossRef]
46. He, J.; He, Y.; Zhuang, J.; Zhang, H.; Lei, B.; Liu, Y. Luminescence properties of Eu^{3+}/CDs/PVA composite applied in light conversion film. *Opt. Mater.* **2016**, *62*, 458–464. [CrossRef]
47. Li, W.; Wu, S.; Xu, X.; Zhuang, J.; Zhang, H.; Zhang, X.; Hu, C.; Lei, B.; Kaminski, C.F.; Liu, Y. Carbon dot-silica nanoparticle composites for ultralong lifetime phosphorescence imaging in tissue and cells at room temperature. *Chem. Mater.* **2019**, *31*, 9887–9894. [CrossRef]
48. Liao, N.; Unnithan, A.R.; Joshi, M.K.; Tiwari, A.P.; Hong, S.T.; Park, C.-H.; Kim, C.S. Electrospun bioactive poly (ϵ-caprolactone)-cellulose acetate-dextran antibacterial composite mats for wound dressing applications. *Colloids Surf. A Physicochem. Eng. Asp.* **2015**, *469*, 194–201. [CrossRef]
49. Shawki, M.M.; Hereba, A.M.; Ghazal, A. Formation and characterisation of antimicrobial dextran nanofibers. *Rom. J. Bio-Phys.* **2010**, *20*, 335–346.
50. Can, H.K.; Kavlak, S.; ParviziKhosroshahi, S.; Guner, A. Preparation, characterization and dynamical mechanical properties of dextran-coated iron oxide nanoparticles (DIONPs). *Artif. Cells Nanomed. Biotechnol.* **2018**, *46*, 421–431. [CrossRef]
51. Bora, A.F.M.; Kouame, K.J.E.-P.; Li, X.; Liu, L.; Sun, Y.; Ma, Q.; Liu, Y. Development, characterization and probiotic encapsulating ability of novel *Momordica charantia* bioactive polysaccharides/whey protein isolate composite gels. *Int. J. Biol. Macromol.* **2023**, *225*, 454–466. [CrossRef] [PubMed]

52. Lekshmi, R.G.K.; Rahima, M.; Chatterjee, N.S.; Tejpal, C.S.; Anas, K.K.; Vishnu, K.V.; Sarika, K.; Asha, K.K.; Anandan, R.; Suseela, M. Chitosan–Whey protein as efficient delivery system for squalene: Characterization and functional food application. *Int. J. Biol. Macromol.* **2019**, *135*, 855–863. [CrossRef] [PubMed]
53. Han, C.; Xiao, Y.; Liu, E.; Su, Z.; Meng, X.; Liu, B. Preparation of Ca-alginate-whey protein isolate microcapsules for protection and delivery of *L. bulgaricus* and *L. paracasei*. *Int. J. Biol. Macromol.* **2020**, *163*, 1361–1368. [CrossRef] [PubMed]
54. Onwulata, C.I.; Isobe, S.; Tomasula, P.M.; Cooke, P.H. Properties of whey protein isolates extruded under acidic and alkaline conditions. *J. Dairy Sci.* **2006**, *89*, 71–81. [CrossRef]
55. Gao, H.; Ma, L.; Li, T.; Sun, D.; Hou, J.; Li, A.; Jiang, Z. Impact of ultrasonic power on the structure and emulsifying properties of whey protein isolate under various pH conditions. *Process. Biochem.* **2019**, *81*, 113–122. [CrossRef]
56. Mine, Y. Recent advances in the understanding of egg white protein functionality. *Trends Food Sci. Technol.* **1995**, *6*, 225–232. [CrossRef]
57. Kim, J.C.; Lund, D.B. Milk protein stainless steel interaction relevant to the initial stage of fouling in thermal processing. *J. Food Process. Eng.* **1998**, *21*, 369–386. [CrossRef]
58. Ge, M.; Li, Y.; Zhu, C.; Liang, G.; Jahangir Alam, S.M.; Hu, G.; Gui, Y.; Junaebur Rashid, M. Preparation of organic-modified magadiite-magnetic nanocomposite particles as an effective nanohybrid drug carrier material for cancer treatment and its properties of sustained release mechanism by Korsmeyer-Peppas kinetic model. *J. Mater. Sci.* **2021**, *56*, 14270–14286. [CrossRef]
59. Wu, I.Y.; Bala, S.; Skalko-Basnet, N.; di Cagno, M.P. Interpreting non-linear drug diffusion data: Utilizing Korsmeyer-Peppas model to study drug release from liposomes. *Eur. J. Pharm. Sci.* **2019**, *138*, 105026. [CrossRef]
60. Nongonierma, A.B.; FitzGerald, R.J. Enhancing bioactive peptide release and identification using targeted enzymatic hydrolysis of milk proteins. *Anal. Bioanal. Chem.* **2018**, *410*, 3407–3423. [CrossRef]
61. Majidiyan, N.; Hadidi, M.; Azadikhah, D.; Moreno, A. Protin complex nanoparticles reinforced with industrial hemp essential oil: Characterization and application for shelf-life extension of rainbow trout fillets. *Food Chem. X* **2022**, *13*, 100202. [CrossRef] [PubMed]
62. Hesami, S.; Safi, S.; Larijani, K.; Badi, H.N.; Abdossi, V.; Hadidi, M. Synthesis and characterization of chitosan nanoparticles loaded with greater celandine (*Chelidonium majus* L.) essential oil as an anticancer agent on MCF-7 cell line. *Int. J. Biol. Macromol.* **2022**, *194*, 974–981. [CrossRef]
63. Ye, Y.Y.; He, J.L.; He, Z.J.; Zhang, N.; Liu, X.Q.; Zhou, J.J.; Cheng, S.Y.; Cai, J. Evaluation of the brewing characteristics, digestion profiles, and neuroprotective effects of two typical Se-enriched green teas. *Foods* **2022**, *11*, 2159. [CrossRef] [PubMed]
64. Anani, J.; Noby, H.; Zkria, A.; Yoshitake, T.; ElKady, M. Monothetic analysis and response surface methodology optimization of calcium alginate microcapsules characteristics. *Polymers* **2022**, *14*, 709. [CrossRef]
65. Wang, P.P.; Li, M.; Wei, D.X.; Ding, M.Z.; Tao, L.N.; Liu, X.W.; Zhang, F.P.; Tao, N.P.; Wang, X.C.; Gao, M.Y.; et al. Electrosprayed soft capsules of millimeter size for specifically delivering fish oil/nutrients to the stomach and intestines. *ACS Appl. Mater. Interfaces* **2020**, *12*, 6536–6545. [CrossRef]
66. Garcia, P.; Vega, J.; Jimenez, P.; Santos, J.; Robert, P. Alpha-tocopherol microspheres with cross-linked and acetylated inulin and their release profile in a hydrophilic model. *Eur. J. Lipid Sci. Technol.* **2013**, *115*, 811–819. [CrossRef]

Disclaimer/Publisher's Note: The statements, opinions and data contained in all publications are solely those of the individual author(s) and contributor(s) and not of MDPI and/or the editor(s). MDPI and/or the editor(s) disclaim responsibility for any injury to people or property resulting from any ideas, methods, instructions or products referred to in the content.